European Journal of Medicinal Chemistry 223 (2021) 113626

Contents lists available at ScienceDirect

European Journal of Medicinal Chemistry

journal homepage: http://www.elsevier.com/locate/ejmech

Noncovalent EGFR T790M/L858R inhibitors based on diphenylpyrimidine scaffold: Design, synthesis, and bioactivity evaluation for the treatment of NSCLC

Lixue Chen [a], Yunhao Zhang [a], Liangliang Tian [b], Changyuan Wang [a], Tuo Deng [b], Xu Zheng [a], Tong Wang [b], Zhen Li [a], Zeyao Tang [a], Qiang Meng [a], Huijun Sun [a], Lei Li [a, *], Xiaodong Ma [a, **], Youjun Xu [b, ***]

[a] College of Pharmacy, Dalian Medical University, Dalian, 116044, PR China
[b] School of Pharmaceutical Engineering, Key Laboratory of Structure-Based Drug Design & Discovery (Ministry of Education), Shenyang Pharmaceutical University, Shenyang, 110016, PR China

ARTICLE INFO

Article history:
Received 19 March 2021
Received in revised form
10 May 2021
Accepted 3 June 2021
Available online 16 June 2021

Keywords:
NSCLC
EGFR T790M/L858R
Resistance
Noncovalent inhibitors

ABSTRACT

A series of diphenylpyrimidine derivatives bearing a hydroxamic acid group was designed and synthesized as noncovalent $EGFR^{T790M/L858R}$ inhibitors to improve the biological activity and selectivity. One of the most promising compound **9d** effectively interfered $EGFR^{T790M/L858R}$ binding with ATP and suppressed the proliferation of H1975 cells with IC_{50} values of 1.097 nM and 0.09777 μM, respectively. Moreover, compound **9d** also not only exhibited a high selective index of 43.4 for $EGFR^{T790M/L858R}$ over the wild-type and 10.9 for H1975 cells over A431, but also exhibited low toxicity against the normal HBE cells (IC_{50} > 20 μM). In addition, the action mechanism validated that compound **9d** effectively inhibited cell migration and promoted cell apoptosis by blocking cell cycle at G_2/M stage. Furthermore, the target dose-dependently downregulated the expression of p-EGFR and arrested the activation of downstream Akt and ERK in H1975. All these studies provide important clues for the discovery of potent noncovalent $EGFR^{T790M/L858R}$ inhibitors.

1. Introduction

EGFR-TK (Epidermal Growth Factor Receptor-Tyrosine Kinase) is an essential enzyme for intracellular signaling and cell transformation, and abnormal activation of EGFR signaling pathway is widespread in many types of solid tumors [1,2], especially in non-small cell lung cancer (NSCLC). Approximately 10–15% non-Asian and 50% Asian patients with NSCLC harbor EGFR activating mutations [3,4]. The majority of EGFR mutations in NSCLC occurs in exons 18–21 of the tyrosine kinase domain of the receptor, such as in-frame deletions in exon 19 (among which the most prominent is del E746_A750, also known as Del 19) or missense mutation in exon 21 (L858R) [5]. Hence, targeting the inhibition of EGFR activation is an effective method to treat lung cancer driven by EGFR-sensitive mutations. Nevertheless, the point mutation of T790 M amino acid enhanced the affinity of EGFR with ATP and then reduced the sensitivity to the first-generation inhibitor (gefitinib, **1**/erlotinib, **2**) (Fig. 1) [6,7]. Based on the structural framework of first-generation inhibitor, covalent irreversible second-generation EGFR inhibitors such as Afatinib (**3**) [8] and Dacomitinib (**4**) [9] have been developed to objectively alleviate the problem of acquired drug resistance caused by T790 M mutation. The acrylamide pharmacophore in the structure reacts with the sulfhydryl group in Cys797 residue (Michael addition reaction) to form a covalent bond that connects the inhibitor to the catalytic region of target enzyme. However, because of its failure to selectively inhibit the mutant EGFR, some side effects were observed, and the application range of second-generation inhibitor was narrowed in clinical trial [10,11]. Excitingly, the third-generation inhibitors, namely, WZ4002 (**5**) [12] and AZD9291 (**6**) [13,14], with the 2-arylamine pyrimidine scaffold exhibited great selective inhibitory effects on $EGFR^{T790M/L858R}$ over Wild-Type EGFR. AZD9291 was approved by the FDA in 2015 for the

* Corresponding author.
** Corresponding author.
*** Corresponding author.
E-mail addresses: lilei0332@126.com (L. Li), xiaodong.ma@139.com (X. Ma), xuyoujun@syphu.edu.cn (Y. Xu).

https://doi.org/10.1016/j.ejmech.2021.113626
0223-5234/

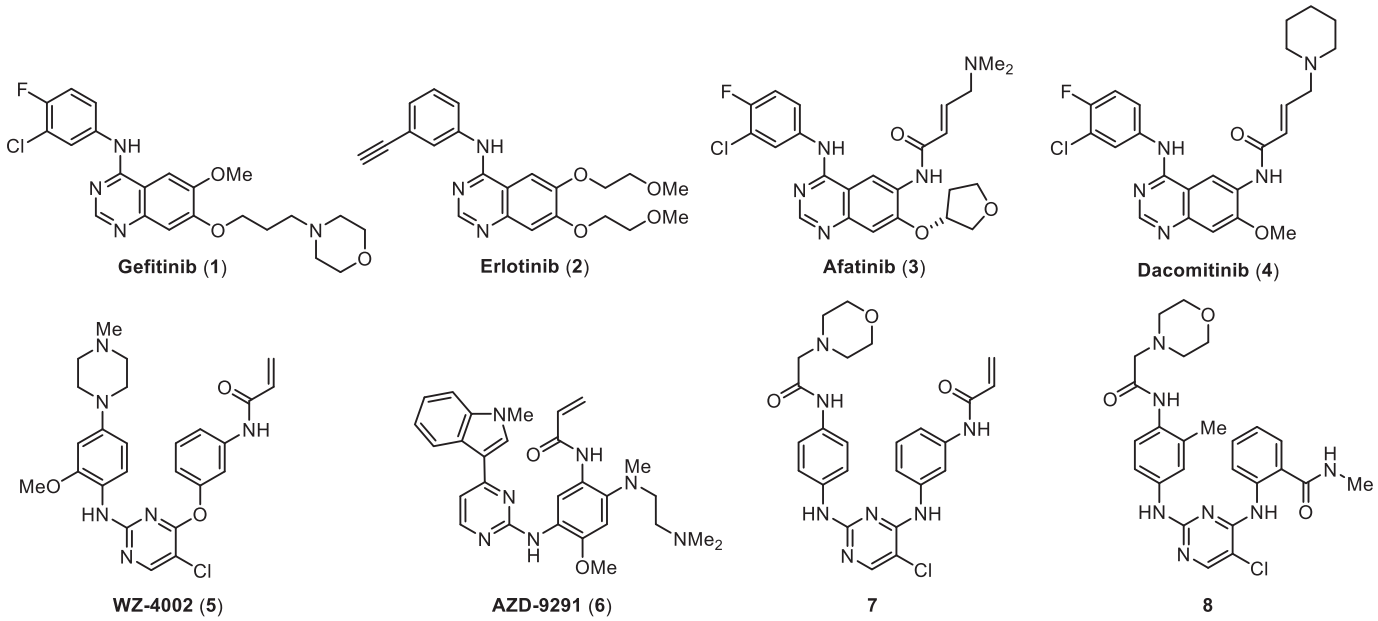

Fig. 1. Chemical structures of some EGFR inhibitors.

treatment of $EGFR^{T790M/L858R}$ mutant lung cancer. With further development of clinical application, approximately 40% [15] of the patients treated with AZD9291 developed a tertiary Cys797 to Ser 797 (C797S) point mutation, thus hindering the covalent bond formation from irreversible inhibitors binding to Cys797 [16,17]. Loss of covalent interaction resulted by C797S mutation causes a significant decrease in the effects of treatment, leading to the development of resistance. Hence, based on the novel 2-arylamine pyrimidine template, it is essential to develop reversible EGFR inhibitors that not only exhibit excellent inhibitory effects on the acquired drug-resistant T790M mutation but also remain potent in other activating mutants [18,19].

Our previous study also validated that this 2-arylamine pyrimidine skeleton has strong activity against a panel of kinases, including FAK [20], JAK3 [21], and BTK [22]. We also synthesized a class of *N*-alkylbenzamide-substituted diphenylpyrimidines based on TAE-226 (FAK inhibitor) [23] and Mor-DPPY (**7**, anti-$EGFR^{T790M/L858R}$) [24] using the fragment-based drug design strategy. Interestingly, the representative compound **8** [20] showed improved inhibitory activity against $EGFR^{T790M/L858R}$ than AZD9291. Although compound **8** only showed moderate antiproliferative activity against H1975 (IC_{50} of 0.333 μM), it provided valuable clues to design potent noncovalent inhibitors against $EGFR^{T790M/L858R}$. In addition, molecular docking studies suggested that double hydrogen bonding interactions were formed between the 2″-amide group of compound **8** and the residues of Asp800. Accordingly, further structural optimization of the hit compound **8** was carried out by introducing a hydroxamic acid group instead of an amide group with an aim to improve the anticancer activity in this study (Fig. 2).

2. Results and discussion

2.1. Chemistry

All the newly designed targets were synthesized as shown in Scheme 1. Commercially available 3-chloropropionyl chloride was reacted with 2-aminobenzoic acid ethyl ester in the presence of a base, DIPEA, to afford **12a** and **12b**. Compounds **13a-k** were then reduced in Argon atmosphere to produce the corresponding products **14a-k** using Zn−NH_4Cl. Moreover, regioselective substitution of the C-2 chlorine atom in **12a** with NH_2 intermediates **14a-h** using TsOH afforded the corresponding products **15a-h**. Finally, the targets **9a-h** were obtained by nucleophilic substitution with hydroxylamine hydrochloride using CH_3ONa. Compounds **9i-k** were also produced using similar methods and conditions. Compound **9l** with two hydroxamic acid groups was obtained by prolonging the reaction time of preparing **9g**. In addition, compound **9m** was synthesized by the hydrolysis reaction of compound **15g**.

2.2. Biological activity

2.2.1. EGFR inhibitory and selective activity assay

Activities of all the targets against $EGFR^{WT}$ and $EGFR^{T790M/L858R}$ were evaluated using ADP-Glo™ kinase assay system. One positive control, AZD9291, was also investigated under the same conditions. The results shown in Table 1 indicate that installing hydroxamic acid on C-2″ position of ring A was an effective method to design noncovalent anti-$EGFR^{T790M/L858R}$ inhibitors. The enzyme-based results show that the designed noncovalent targets displayed strong inhibitory activities against the $EGFR^{T790M/L858R}$ with IC_{50} ranging from 0.2446 to 198.5 nM. Among them, compounds **9d** (IC_{50} = 1.097 nM) and **9e** (IC_{50} = 6.820 nM) showed stronger affinity to $EGFR^{T790M/L858R}$ than AZD9291 (IC_{50} = 20.80 nM). Some compounds **9d** and **9g** showed selective inhibitory effects on $EGFR^{T790M/L858R}$ over Wild-Type EGFR, indicating their weak interference with the expression of $EGFR^{WT}$. It was observed that the linker installed between rings C and D clearly effected the activities; the substitution of linear carbon units was the most helpful in inhibiting the $EGFR^{T790M/L858R}$ binding with ATP, such as compounds **9d** and **9e**. Compared with *N*-methylpiperazinyl group, compound **9d** substituted with a morpholinyl group exhibited excellent selectivity with an SI of 47. When a hydroxamic acid group was installed on ring D, compounds **9i**, **9j**, and **9k** showed weak inhibitory activities against $EGFR^{T790M/L858R}$ in spite of replacing the linker with 0−3 carbon units. Compound **9l** with two hydroxamic acid groups exhibited moderate anti-$EGFR^{T790M/L858R}$ activity without selectivity. Notably, the ester-substituted compound

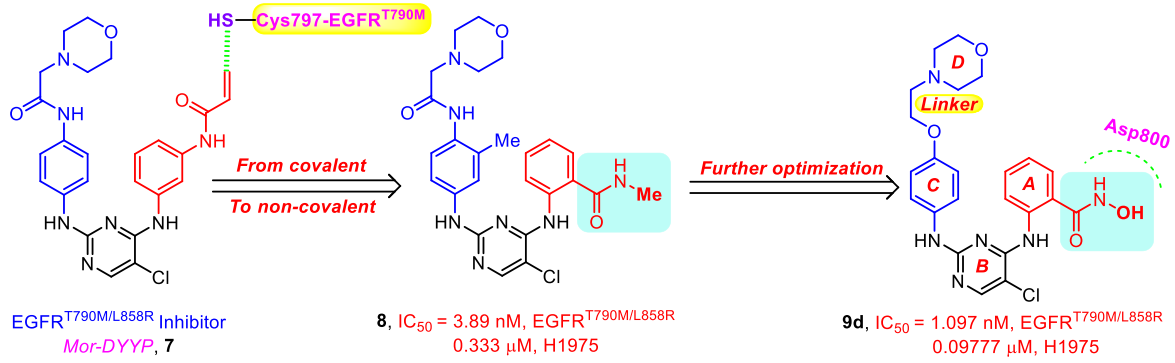

Fig. 2. Design strategy of title compounds.

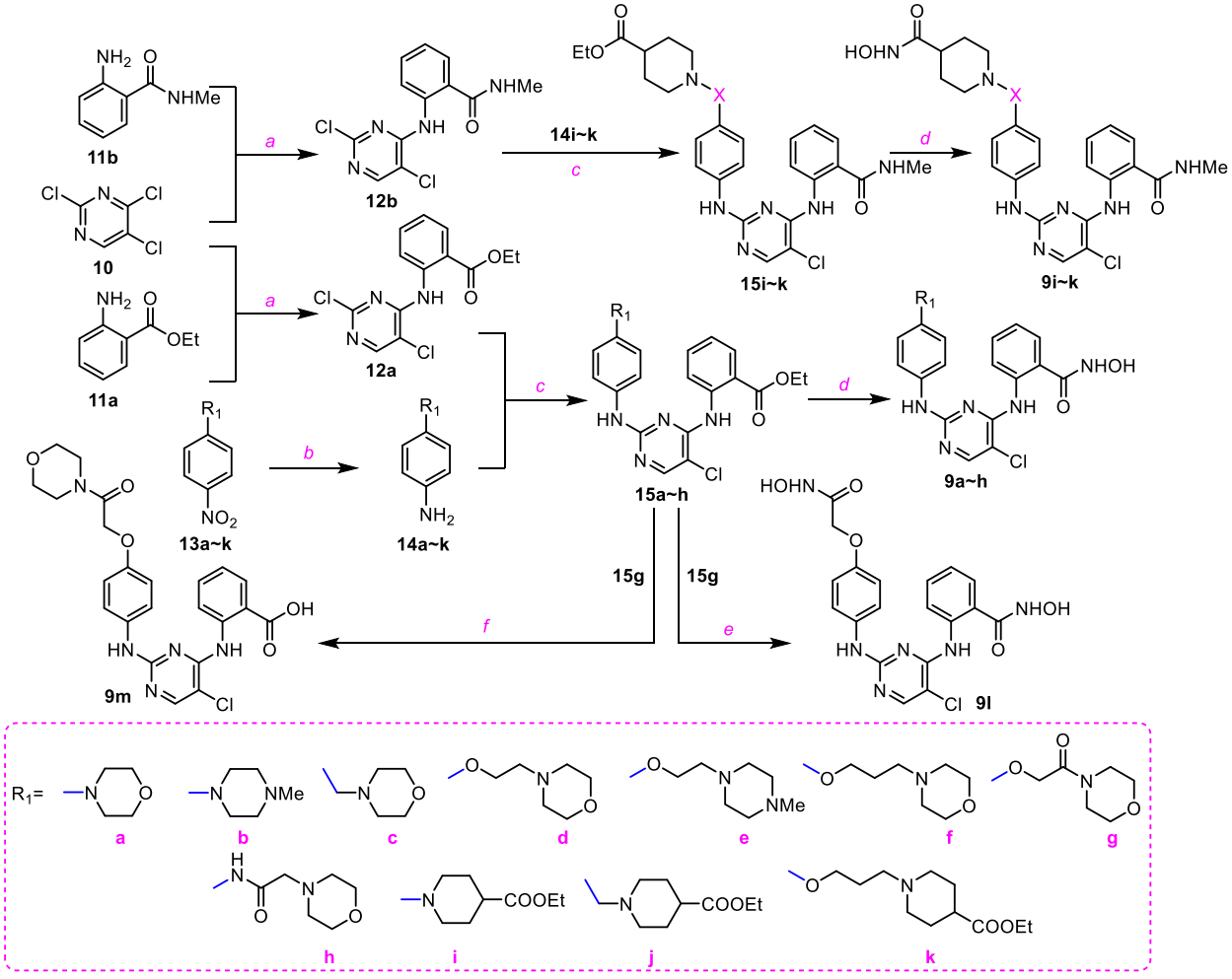

Reagents and conditions: a. DIPEA in CH_3CN, 80 °C for 10 h 95.6%, 96.3%. b. Zn, aq. NH_4Cl in EtOH, from rt to 70 °C for 1 h, 82.5~93.2%. (c) TsOH in EtOH, 70 °C for 5 h, 55.3~63.6%; (d) NH_2OH HCl, CH_3ONa in MeOH, from ice–bath to rt for 2~3 h, 55.0~69.8%. e. H_2NOH HCl, NaOMe in MeOH, rt for 10 h, 69.6%. f. aq. NaOH in 1,4-dioxane, rt, then aq. HCl, 62.1%.

Scheme 1. Synthetic route of targets **9a–m**, **15g**.

(prodrug form of carboxylic acid) **15g** also showed strong kinase inhibitory activity, and it is worthy for further evaluation.

2.2.2. Cellular inhibitory and selective activity assay

The antiproliferative activities of the targets and positive control AZD9291 were studied by conducting a CCK-8 assay in NSCLC cell lines A431-EGFR^{WT}, H1975-EGFR$^{T790M/L858R}$, A549-KRAS^{G12S}, and H23 KRAS^{mutant}, one human metastatic pancreatic adenocarcinoma cell line (Aspc-1), and one normal cell line (HBE). The results shown in Table 2 indicate that all the targets showed strong inhibitory activity against H1975 with IC$_{50}$ < 1.11 μM. Compounds **9b** and **9c** (IC$_{50}$ < 0.0781 μM) showed more activity than AZD9291

Table 1
EGFR tyrosine kinase inhibitory activities of **9a-m**, **15g** *in vitro*[a].

.

Compd.	R_1	R_2	Enzymatic activity (IC_{50}, nM)	
			$EGFR^{T790M/L858R}$	$EGFR^{WT}$
9a		-CONHOH	116.5 ± 5.68	168.7 ± 7.21
9b		-CONHOH	68.81 ± 2.31	6.564 ± 1.23
9c		-CONHOH	98.78 ± 1.56	4.495 ± 0.56
9d	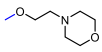	-CONHOH	1.097 ± 0.47	47.66 ± 3.20
9e	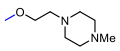	-CONHOH	6.82 ± 1.14	0.7632 ± 0.04
9f	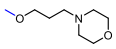	-CONHOH	64.79 ± 4.69	1.246 ± 0.48
9g	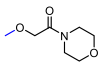	-CONHOH	16.04 ± 1.56	57.31 ± 2.35
9h	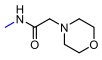	-CONHOH	113.5 ± 6.51	126.0 ± 5.24
9i	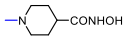	-CONHMe	49.94 ± 5.65	118.7 ± 4.52
9j	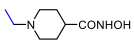	-CONHMe	117.5 ± 3.21	1.095 ± 0.26
9k	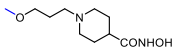	-CONHMe	44.96 ± 2.50	46.69 ± 4.32
9l	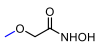	-CONHOH	65.41 ± 3.22	50.22 ± 5.20
9m	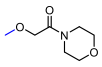	-COOH	198.5 ± 6.78	81.40 ± 2.31
15g	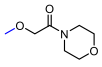	-COOEt	0.2446 ± 0.04	32.00 ± 1.58
AZD9291	–	–	20.80 ± 2.22	567.5 ± 6.57

[a] Dose-response curves were determined at three concentrations. The IC_{50} values are the concentrations in nanomolar level needed to inhibit the cell growth by 50% as determined from these curves.

(IC_{50} = 0.091 μM). Compounds **9a** (IC_{50} = 0.1093) and **9d** (IC_{50} = 0.09777 μM) showed equivalent potency against proliferation compared with the positive drug. Several of the targets, **9a**, **9c**, and **9d**, showed high selective antiproliferative activity against H1975 over A431 (SI > 10), indicating their weak side effects. Meanwhile, the targets also showed strong inhibitory activity against A549, H23 bearing k-ras mutant tumor cells, and ASCP-1 with the values of IC_{50} in nanomolar level. However, these inhibitors are not sensitive to the normal HBE cells with concentrations of up to 8.566 μM, indicating their low cytotoxicity. The SAR analysis of targets indicates that when ring D was substituted with a morpholinyl group, one carbon unit linker between rings C and D was the most effective for the activity and selectivity than by extending or shortening the linker (**9c**, IC_{50} < 0.0781 μM). The substitution of ring D with an *N*-methylpiperazinyl group, **9b**, with rings C and D connected directly, showed the highest activity (IC_{50} < 0.0781 μM). When replacing the linker with an acetamide linker, compounds **9g** and **9h** exhibited moderate inhibitory activity against H1975, with IC_{50} values of 0.1291 μM and 0.3846 μM, respectively. It is also not conducive for antitumor activity when ring D is replaced with a hydroxamic acid group (**9l**, IC_{50} = 1.110 μM). In addition, the yield of targets **9m** (IC_{50} > 10 μM) and **15g** (IC_{50} = 2.905 μM) without the substitution of hydroxamic acid group at the C-2″ position of ring A showed a significant decrease against inhibiting the proliferation of cells, further confirming the rationality of the design strategy. Notably, compounds **9b** or **9c** showed strong inhibitory activity and selectivity against H1975, but their hepatotoxicity prevented the possibility of further study of the target. According to the test results of activity, selectivity, and toxicity, compound **9d** was selected as the candidate for further mechanism research.

2.2.3. Migration inhibition assay

A wound-healing assay, as shown in Fig. 3, was preformed to evaluate the inhibition of migration of H1975. After scratching the cell monolayer, H1975 cells were exposed to different concentrations of 0.5 and 2 μM for 0, 24, and 48 h. The negative control group demonstrated the strongest migratory ability, and the width of the scratch was significantly narrowed. As expected, the transfer of cell numbers to the scratch in the compound **9d**-treated groups was obviously less than the negative control group. The evaluation of wound-healing assay indicated that the migration and invasion of H1975 cells were effectively inhibited by compound **9d**.

2.2.4. Morphological staining analysis

DAPI staining was carried out to observe the morphological changes in H1975 cells exposed with compound **9d** in different concentrations of 0.5 and 2.0 μM for 48 h. As shown in Fig. 4A, subsequent to DAPI staining, chromatin shrinks as well as gathering towards the nuclear membrane were clearly observed. With the increase in concentration, the nucleus was disintegrated to from fragments. Under natural lights, the proportion of abnormal cells such as fusiform and sickle type increased significantly (Fig. 4B). All the phenomena indicate the characteristics of apoptotic programmed cell death.

2.2.5. Flow cytometry analysis

To gain an in-depth understanding of mechanism of action, the apoptosis and cycle of H1975 cells treated with compound **9d** were evaluated by flow cytometry analysis. The analysis results show that after exposure with compound **9d** in different concentrations of 0.125, 0.5, and 2 μM for 48 h, the apoptosis rate of H1975 cells increased from 4.31% to 91.22% in a dose-dependent manner (Fig. 5A). Correspondingly, the effect of compound **9d** on cell cycle progression is shown in Fig. 5B. When exposed with the dosage of 0.125 μM, the percentage of G_1/G_0 phase significantly decreased from 58.05% to 20.25%. The percentage of G_2/M phase increased from 30.23% to 64.66%, and the percentage of S phase increased from 11.72% to 15.08% as well. With the increase in concentration to 0.5 μM, conversely, the proportion of S phase decreased to 9.86%, and the proportion of G_2/M phase further increased up to 70.99%. Notably, when the concentration of exposure was further increased to 2.0 μM, the machine failed to capture the process of blocking cell division due to a large number of dead cells left (Table 3). Flow cytometric analysis indicated that compound **9d** induced the apoptosis of H1975 by arresting the cell cycle at the G_2/M stage.

2.2.6. Effects of the inhibitors on $EGFR^{T790M/L858R}$ activation and downstream signaling

With strong kinase and cellular inhibitory activities, compound **9d** was further validated by evaluating its potential suppression on the activity of $EGFR^{T790M/L858R}$ and downstream signaling in H1975 cells. The cells were exposed with compound **9d** in various

Table 2
Cellular antiproliferative activities of **9a-m** and **15g** (IC_{50}, μM).

Compd.	Anti-proliferative activity (IC_{50}, μM)							SI
	H1975	A431	A549	HBE	ASPC-1	H23	L-02	
9a	0.1093 ± 0.09	1.581 ± 0.22	0.1093 ± 0.13	>40	1.410 ± 0.23	0.8007 ± 0.05	2.191 ± 0.23	14.46
9b	<0.0781	0.2532 ± 0.07	<0.078	22.59 ± 1.58	<0.156	0.2173 ± 0.05	<1.25	>3.24
9c	<0.0781	2.427 ± 0.12	<0.078	29.11 ± 1.23	<0.156	0.5537 ± 0.06	<1.25	>31.08
9d	0.09777 ± 0.02	1.066 ± 0.10	0.0977 ± 0.03	23.61 ± 0.78	0.1691 ± 0.05	0.6249 ± 0.09	3.052 ± 0.56	10.90
9e	0.8218 ± 0.05	0.6916 ± 0.06	0.2028 ± 0.01	29.83 ± 1.25	0.2442 ± 0.05	0.6425 ± 0.07	1.9494 ± 0.97	0.84
9f	0.3209 ± 0.07	1.404 ± 0.11	0.3209 ± 0.05	26.51 ± 2.21	1.229 ± 0.12	0.665 ± 0.09	1.733 ± 0.55	4.38
9g	0.1291 ± 0.07	0.6698 ± 0.03	0.1291 ± 0.06	20.21 ± 0.78	0.5302 ± 0.06	0.8195 ± 0.06	4.814 ± 0.87	5.19
9h	0.3846 ± 0.06	1.532 ± 0.11	0.3846 ± 0.07	>40	0.7498 ± 0.04	1.74 ± 0.06	2.114 ± 0.56	3.98
9i	0.3289 ± 0.03	0.1271 ± 0.06	0.3289 ± 0.07	12.65 ± 0.23	0.4994 ± 0.02	1.541 ± 0.07	1.733 ± 0.55	0.39
9j	0.245 ± 0.04	1.156 ± 0.12	0.245 ± 0.09	15.93 ± 0.32	0.3741 ± 0.02	8.425 ± 1.10	1.278 ± 0.80	4.72
9k	0.1556 ± 0.07	0.4482 ± 0.04	0.1556 ± 0.02	8.566 ± 0.58	<0.156	2.114 ± 0.21	<1.25	2.88
9l	1.11 ± 0.11	2.065 ± 0.23	1.11 ± 0.09	>40	1.577 ± 0.36	6.397 ± 0.98	7.869 ± 0.40	1.86
9m	>10	–	–	–	–	–	15.51 ± 1.25	–
15g	2.905 ± 0.23	–	–	–	–	–	30.22 ± 2.32	–
AZD9291	0.091 ± 0.01	1.226 ± 0.12	–	–	–	–	–	–

a Dose-response curves were determined at five concentrations. The IC_{50} values are the concentrations in micromolar level needed to inhibit the cell growth by 50% as determined from these curves.

concentrations (0.5 and 1.0 μM) for 24 h, and then the levels of p-$EGFR^{T790M/L858R}$, p-AKT and p-ERK were determined by immunoblotting analysis. The results shown in Fig. 6 show that the expression of p-EGFRT790 M/L858R decreased after administration of 9d with the concentration of 0.5 μM. Correspondingly, the phosphorylation of AKT and ERK, which acted downstream of the signaling pathway, was also inhibited significantly. When the dosage was increased to 1.0 μM, the expression of p-EGFR as well as p-Akt and p-ERK further decreased in a dose-dependent manner. Similar results were obtained in H1975 cells treated with AZD9291 at concentrations from 0.5 to 1.0 μM. These results indicated that 9d could block the autophosphorylation of EGFR and then inhibited the activation of the downstream signaling kinases.

2.2.7. Pharmacokinetic studies

After intravenous injection of **9d** in SD rats, the pharmacokinetic parameters and curve of the blood drug concentration−time and are shown in Table 4 and Fig. 7. The drug concentration declined rapidly within 12 h, the elimination half-life was 9.51 h. Strikingly, the area under the drug time curve of **9d** ($AUC_{(0-\infty)}$) was

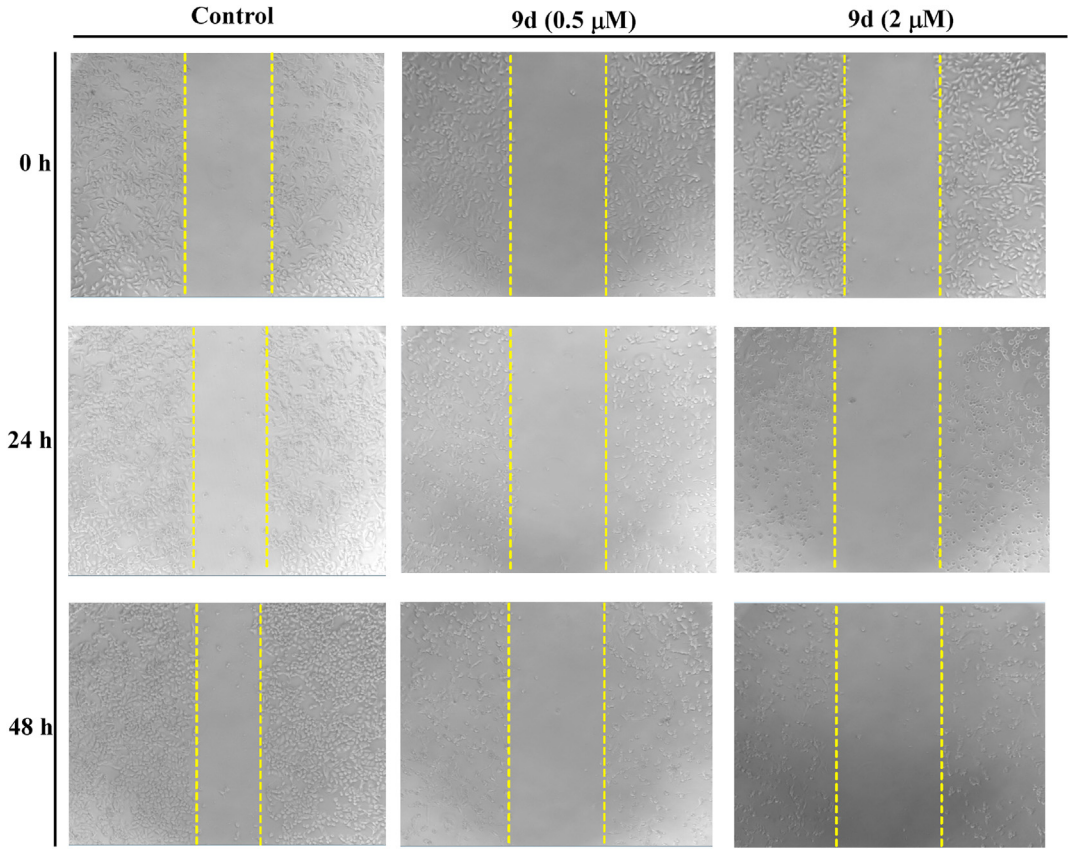

Fig. 3. Representative images of H1975 cells treated with different concentrations of **9d** for 0, 24, and 48 h by the wound-healing assay.

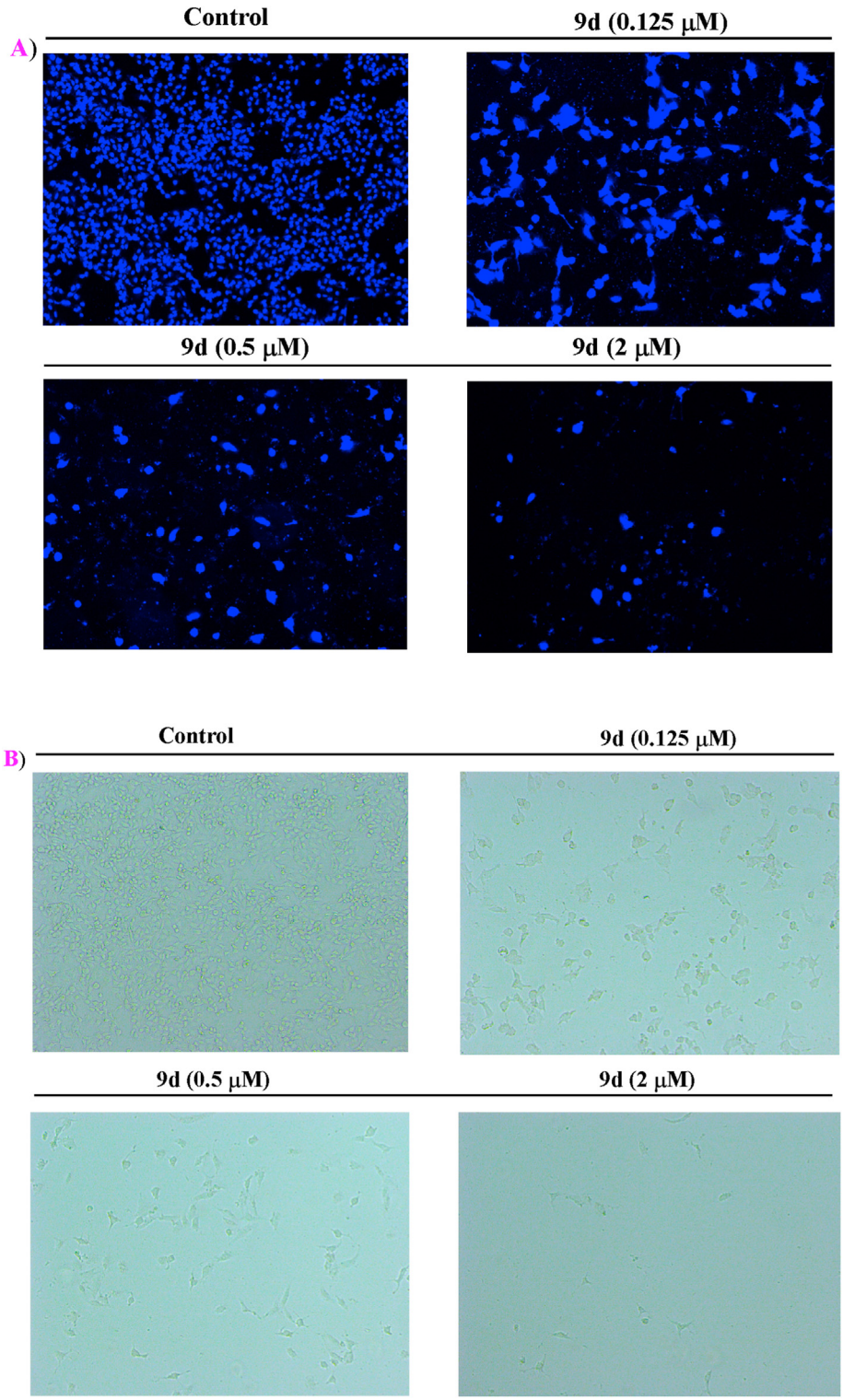

Fig. 4. Morphological changes in H 1975 cells (100 ×, final magnification). A): DAPI staining of H 1975 cells treated with different concentrations of compound **9d** for 72 h. B): Under natural light, H1975 cells treated with different concentrations of compound **9d** for 72 h.

45192.58 μg/L*h. Meanwhile, the mean residence time $MRT_{(0-\infty)}$ of **9d** was 13.13 h.

2.3. Molecular modelling analysis

The crystal complex (PDB code: 3IKA) of WZ4002 binding to the catalytic site of $EGFR^{T790M/L858R}$ kinase as a model, the binding mode of compound **9d** with $EGFR^{T790M/L858R}$, was elucidated using AutoDock 4.2 software. The results of docking study indicate that compound **9d** exactly occupied the site of ATP-binding pocket in a U-shape, but the binding conformation of compound **9d** was reversed to that of WZ4002. The interactions between compound

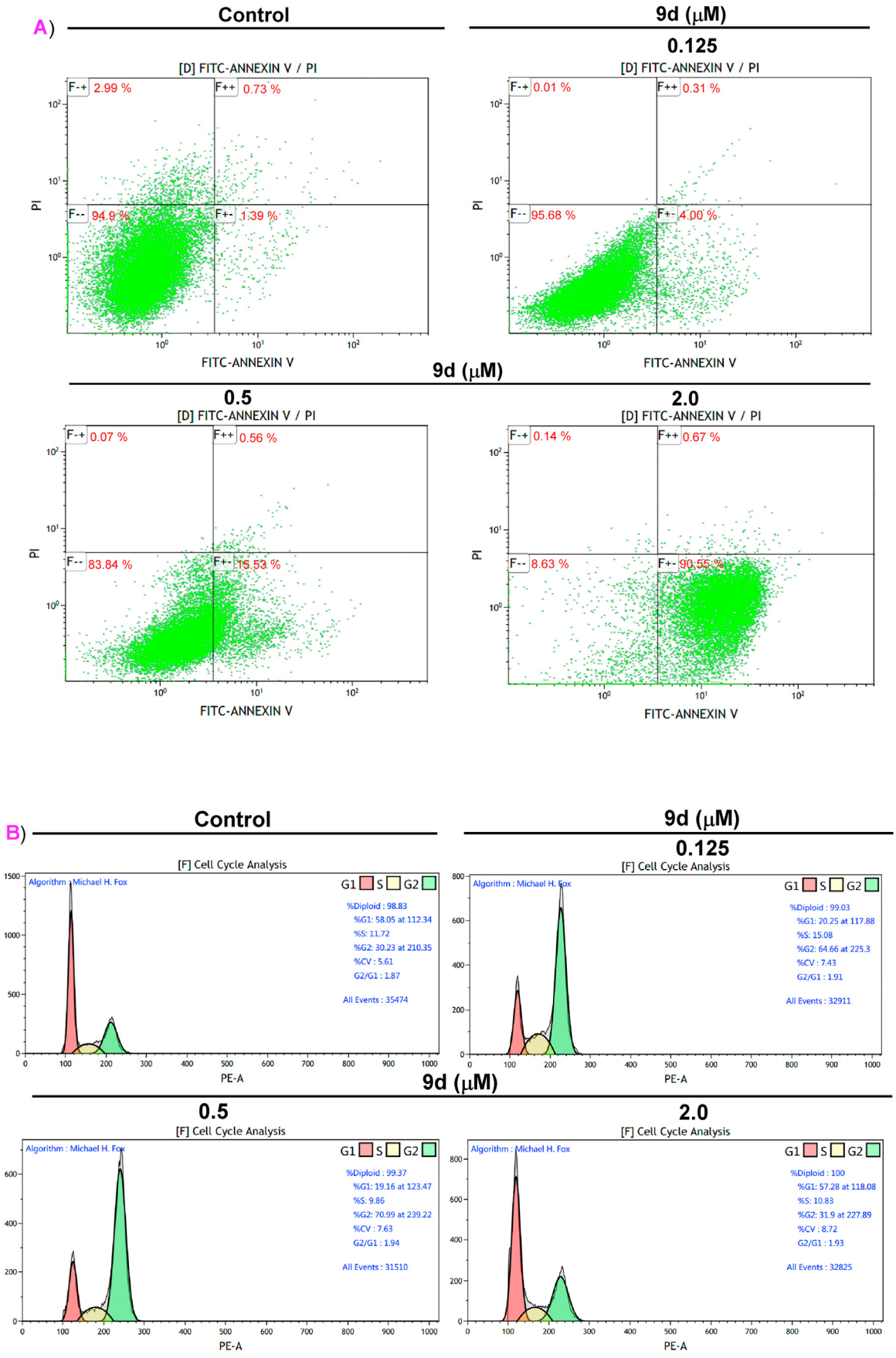

Fig. 5. A) Compound **9d** induced H1975 cells apoptosis *in vitro*. B) Effects of compound **9d** on H1975 cycle arrest were detected by flow cytometry assay.

Table 3
The change of cell cycle and apoptotic proportion of H1975 cells after administration of **9d** (%).

	G_1/G_0	S	G_2/M	Necrotic cells	Viable apoptosis	Non-viable apoptosis
CON.	58.05	11.72	30.23	2.99	0.73	1.39
0.125 μM	20.25	15.08	64.66	0.01	0.31	4.00
0.5 μM	19.16	9.86	70.99	0.07	0.56	15.53
2.0 μM	57.28	10.83	31.90	0.14	0.67	90.55

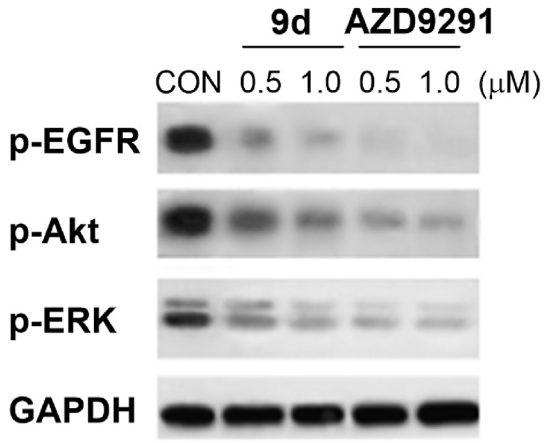

Fig. 6. Compound **9d** inhibited the autophosphorylation of $EGFR^{T790M/L858R}$ and activation of its downstream signaling proteins (A) and grayscale analysis (B) in H1975 cells.

Table 4
Pharmacokinetic parameters of **9d** after intravenous administration.

	9d
$AUC_{(0-t)}$ (μg/L*h)	37632.19 ± 1244.71
$AUC_{(0-\infty)}$ (μg/L*h)	45192.58 ± 2100.40
$MRT_{(0-t)}$ (h)	8.196 ± 0.213
$MRT_{(0-\infty)}$ (h)	13.13 ± 0.75
$t_{1/2z}$ (h)	9.51 ± 0.48
CL_z (L/h/kg)	0.554 ± 0.03

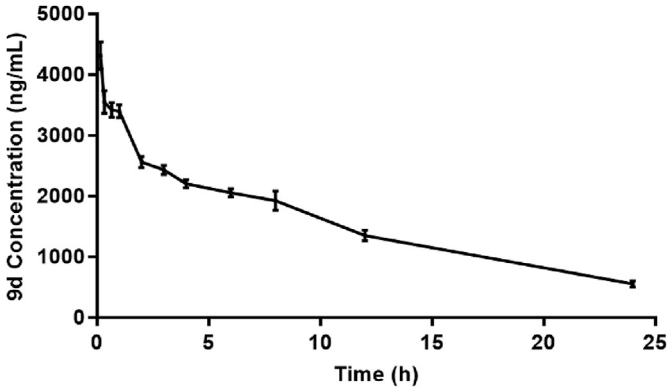

Fig. 7. Drug concentration-time curve of **9d**.

9d and $EGFR^{T790M/L858R}$ included two parts: 1) The hydroxamic acid functional group of the molecule formed two hydrogen bonds with Asp800 residue, and another strong hydrogen bond was established between the 2-amino group in the pyrimidine core of compound **9d** and Met 793 in the kinase hinge. The hydrogen bonding forces were envisioned to be important for improving the affinity of enzyme binding the target over ATP. 2) Several van der Waals interactions existed between compound **9d** and the residues of protein, such as ring A with Leu 718 and ring C and D with Leu 844 (Fig. 8). The docking model combined with the data obtained from the biological assays provided a structural basis for further development of noncovalent $EGFR^{T790M/L858R}$ inhibitors.

3. Conclusion

Replacement of the acrylamide group with an *N*-methylformyl group installed on the C-2″ position of 4-aniline in WZ4002 provided a significant method for designing noncovalent $EGFR^{T790M/L858R}$ inhibitors and a desirable starting point for further optimization. A class of diphenylpyrimidine derivatives bearing a hydroxamic acid functionality was synthesized as effective noncovalent $EGFR^{T790M/L858R}$ inhibitors. Among them, several compounds not only showed strong inhibitory activity against $EGFR^{T790M/L858R}$ and selectivity of binding the receptor, but also displayed high antiproliferative activity against H1975 cells. Furthermore, these inhibitors induced remarkable apoptosis in H1975 cells by blocking the cell cycle at the G_2/M stage, as well as inhibited the activation of EGFR and its downstream pathways. Overall, all these studies provide a new insight to discover novel noncovalent inhibitors for the treatment of NSCLC harboring $EGFR^{T790M/L858R}$ mutation.

4. Experimental section

4.1. General methods and chemistry

Unless otherwise noted, commercial solvents and reagents were used without further purifications. High resolution ESI-MS was performed on an Agilent 1100 HPLC/MS system. ^{1}H NMR and ^{13}C NMR spectra on a Brucker AV 400 MHz spectrometer were recorded in DMSO-d_6. Coupling constants (J) are expressed in hertz (Hz). Chemical shifts (d) of NMR are reported in parts per million (ppm) units relative to internal control (TMS). All reactions were monitored by TLC, using silica gel plates with fluorescence GF254 and UV light visualization. Flash chromatography separations were obtained on Silica Gel (300–400 mesh) using dichloromethane/methanol as eluents.

4.2. General procedure for the synthesis of ***9a-m***

11a-b (50 mmol), 2,4,5-trichloropyrimidine (50 mmol) and DIPEA (100 mmol) in acetonitrile, it was gradually heated to 80 °C and stirred for 10 h. The precipitate was filtrated and washed with water, and the acquired production could directly be used without further purification. **13a-k** was prepared according to the reported process [20–22,24]. Ar atmosphere, a mixture of **13a-k** (15 mmol), ammonium chloride (20 mmol) and zinc powder (120 mmol) in ethanol/water (100/20 mL) was reacted at 70 °C for 1 h. After the reaction, the solvent was distilled off and the residue was dispersed in dichloromethane. The zinc powder was removed by filtration, and the organic layer was washed with dilute ammonia and dried over anhydrous sodium sulfate. The organic was vacuum distilled to

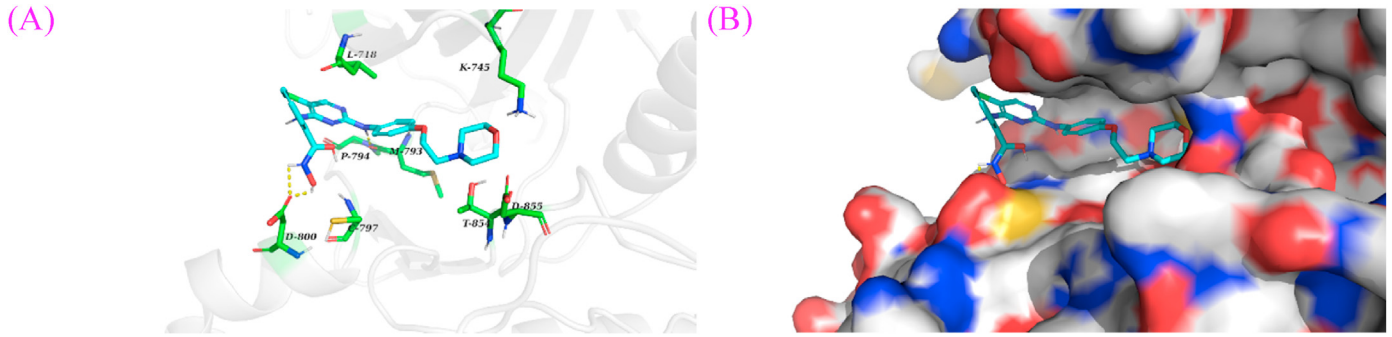

Fig. 8. Putative binding mode of **9d** with $EGFR^{T790M/L858R}$. (A) Detailed interactions with the protein residues. Each dashed yellow line represents hydrogen bonds. (B) Three-dimensional space matching diagram of **9d** and the active site.

give the crude which was purified by silica-gel column separation to get the **14a**-**k**.

A mixture of **12a**-**b** (5.0 mmol), **14a**-**k** (5.0 mmol), and *p*-TsOH (7.5 mmol) in ethyl alcohol was gradually heated to 70 °C and stirred for 3 h. After reaction, the solvent was vacuum distilled and the residuum was dispersed with saturated sodium bicarbonate/ethyl acetate. The crude product was purified using flash chromatography with dichloromethane/methanol as eluents.

Ar atmosphere, **15a**-**k** (2.0 mmol) and hydroxylamine (40 mmol) in anhydrous methanol, sodium methoxide (25 mmol) in methanol solution was slowly added to the mixture. After the addition, the reaction was allowed to warm room temperature and stirred for 2 h. Adjusted pH to 6 with dilute hydrochloric acid, the inorganic salt was removed by filtration and the rest of organic phase was vacuum distilled to produce the **9ã k**.

*4.2.1. 2-((5-chloro-2-((4-morpholinophenyl)amino)pyrimidin-4-yl) amino)-N-hydroxy benzamide (**9a**)*

Yield 65.2%; off-white solid; dichloromethane/methanol: 10/1 (v/v). ^{1}H NMR (400 MHz, DMSO–d_6): δ 11.51 (s, 1H), 11.17 (s, 1H), 9.34 (s, 1H), 9.26 (s, 1H), 8.71 (s, 1H), 8.17 (s, 1H), 7.61(dd, J = 7.84, 1.14 Hz, 1H), 7.49−7.47 (m, 3H), 7.12(td, J = 7.83, 0.84 Hz, 1H), 6.89 (d, J = 8.89 Hz, 2H), 3.74 (t, J = 4.92 Hz, 4H), 3.05 (t, J = 4.62 Hz, 4H); ^{13}C NMR (100 MHz, DMSO–d_6): δ 166.34, 158.48, 155.36, 155.14, 147.01, 139.61, 132.92, 131.98, 128.01, 122.48, 121.99, 121.75 (2C), 119.54, 115.97 (2C), 104.65, 66.65, 49.72. HRMS (ESI^+) for $C_{21}H_{21}ClN_6O_3$, $[M+H]^+$ calcd: 441.1436, found: 441.1409.

*4.2.2. 2-((5-chloro-2-((4-(4-methylpiperazin-1-yl)phenyl)amino) pyrimidin-4-yl)amino)-N-hydroxy benzamide (**9b**)*

Yield 62.3%; off-white solid; dichloromethane/methanol: 10/1 (v/v). ^{1}H NMR (400 MHz, DMSO–d_6): δ 11.17 (s, 1H), 9.23 (s, 1H), 8.71 (s, 1H), 8.17 (s, 1H), 7.61(dd, J = 7.75, 0.96 Hz, 1H), 7.48−7.46 (m, 3H), 7.11(td, J = 7.59, 0.78 Hz, 1H), 6.87 (d, J = 9.00 Hz, 2H), 3.08 (t, J = 4.62 Hz, 4H), 2.49 (t, J = 4.60 Hz, 4H), 2.24 (s, 3H); ^{13}C NMR (100 MHz, DMSO–d_6): δ 166.24, 158.52, 155.34, 155.16, 146.98, 139.60, 132.61, 131.93, 127.99, 122.43, 121.95 (2C), 121.77, 119.51, 116.20 (2C), 104.58, 55.07 (2C), 49.19 (2C), 46.10. HRMS (ESI^+) for $C_{22}H_{24}ClN_7O_2$, $[M+H]^+$ calcd: 454.1753, found: 454.1730.

*4.2.3. 2-((5-chloro-2-((4-(morpholinomethyl)phenyl)amino) pyrimidin-4-yl)amino)-N-hydroxy benzamide (**9c**)*

Yield 56.4%; off-white solid; dichloromethane/methanol: 12/1 (v/v). ^{1}H NMR (400 MHz, DMSO–d_6): δ 11.18 (s, 1H), 9.46 (s, 1H), 8.70 (s, 1H), 8.22 (s, 1H), 7.63−7.59 (m, 3H), 7.47 (t, J = 7.27 Hz, 1H), 7.18 (d, J = 7.92 Hz, 2H), 7.13 (t, J = 7.26 Hz, 1H), 3.57−3.54 (m, 4H), 3.39 (s, 2H), 2.36−2.31 (m, 4H); ^{13}C NMR (100 MHz, DMSO–d_6): δ 166.23, 158.28, 155.44, 155.16, 139.57, 139.49, 131.87, 131.38, 129.62 (2C), 128.08, 122.65, 122.19, 120.09 (2C), 119.84, 105.39, 66.68 (2C), 62.58, 53.58 (2C). HRMS (ESI^+) for $C_{22}H_{23}ClN_6O_3$, $[M+H]^+$ calcd: 455.1593, found: 455.1564.

*4.2.4. 2-((5-chloro-2-((4-(2-morpholinoethoxy)phenyl)amino) pyrimidin-4-yl)amino)-N-hydroxy benzamide (**9d**)*

Yield 61.2%; off-white solid; dichloromethane/methanol: 12/1 (v/v). ^{1}H NMR (400 MHz, DMSO–d_6): δ 11.51 (s, 1H), 11.16 (s, 1H), 9.35 (s, 1H), 9.30 (s, 1H), 8.69 (s, 1H), 8.18 (s, 1H), 7.61 (d, J = 7.68 Hz, 1H), 7.51 (d, J = 8.52 Hz, 2H), 7.48 (t, J = 8.28 Hz, 1H), 7.11 (t, J = 7.32 Hz, 1H), 6.87 (d, J = 8.94 Hz, 2H), 4.06 (t, J = 5.70 Hz, 2H), 3.59 (t, J = 3.96 Hz, 4H), 2.71−2.68 (m, 2H), 2.50−2.42 (m, 4H); ^{13}C NMR (100 MHz, DMSO–d_6): δ 166.23, 158.45, 155.37, 155.17, 154.18, 139.54, 133.77, 131.92, 128.02, 122.50, 122.06 (2C), 122.01, 119.63, 114.80 (2C), 104.80, 66.55 (2C), 65.85, 57.53, 54.07 (2C). HRMS (ESI^+) for $C_{23}H_{25}ClN_6O_4$, $[M+H]^+$ calcd: 485.1699, found: 485.1673.

*4.2.5. 2-((5-chloro-2-((4-(2-(4-methylpiperazin-1-yl)ethoxy) phenyl)amino)pyrimidin-4-yl)amino)-N-hydroxybenzamide (**9e**)*

Yield 62.3%; off-white solid; dichloromethane/methanol: 10/1 (v/v). ^{1}H NMR (400 MHz, DMSO–d_6): δ 11.16 (s, 1H), 9.29 (s, 1H), 8.68 (s, 1H), 8.18 (s, 1H), 7.61 (d, J = 7.62 Hz, 1H), 7.51 (d, J = 8.28 Hz, 2H), 7.48 (t, J = 7.68 Hz, 1H), 7.11 (t, J = 7.44 Hz, 1H), 6.86 (d, J = 8.82 Hz, 2H), 4.03 (t, J = 5.76 Hz, 2H), 3.42−3.40 (m, 4H), 2.66 (t, J = 5.70 Hz, 2H), 2.38−2.27 (m, 4H), 2.16 (s, 3H); ^{13}C NMR (100 MHz, DMSO–d_6): δ 166.20, 158.46, 155.37, 155.16, 154.25, 139.53, 133.72, 131.89, 128.01, 122.49, 122.09 (2C), 122.01, 119.66, 114.78 (2C), 104.79, 66.19, 57.14, 55.13 (2C), 53.43 (2C), 46.13. HRMS (ESI^+) for $C_{24}H_{28}ClN_7O_3$, $[M+H]^+$ calcd: 498.2015, found: 498.1997.

*4.2.6. 2-((5-chloro-2-((4-(3-morpholinopropoxy)phenyl)amino) pyrimidin-4-yl)amino)-N-hydroxy benzamide (**9f**)*

Yield 55.0%; off-white solid; dichloromethane/methanol: 12/1 (v/v). ^{1}H NMR (400 MHz, DMSO–d_6): δ 11.51 (s, 1H), 11.16 (s, 1H), 9.37 (s, 1H), 9.29 (s, 1H), 8.69 (s, 1H), 8.18 (s, 1H), 7.61 (d, J = 7.62 Hz, 1H), 7.50 (d, J = 8.52 Hz, 2H), 7.47 (t, J = 7.62 Hz, 1H), 7.11 (t, J = 7.56 Hz, 1H), 6.85 (d, J = 8.94 Hz, 2H), 3.97 (t, J = 6.30 Hz, 2H), 3.57 (t, J = 4.14 Hz, 4H), 2.42 (t, J = 7.08 Hz, 2H), 2.39−2.36 (m, 4H), 1.88−1.84 (m, 2H); ^{13}C NMR (100 MHz, DMSO–d_6): δ 166.22, 158.48, 155.37, 155.17, 154.41, 139.55, 133.65, 131.90, 128.02, 122.48, 122.14 (2C), 122.00, 119.62, 114.76 (2C), 104.80, 66.63 (2C), 66.40, 55.38, 53.82 (2C), 26.39. HRMS (ESI^+) for $C_{24}H_{27}ClN_6O_4$, $[M+H]^+$ calcd: 499.1855, found: 499.1837.

*4.2.7. 2-((5-chloro-2-((4-(2-morpholino-2-oxoethoxy)phenyl) amino)pyrimidin-4-yl)amino)-N-hydroxybenzamide (**9g**)*

Yield 56.3%; off-white solid; dichloromethane/methanol: 12/1 (v/v). ^{1}H NMR (400 MHz, DMSO–d_6): δ 11.50 (s, 1H), 11.17 (s, 1H),

9.34 (s, 1H), 9.30 (s, 1H), 8.70 (s, 1H), 8.18 (s, 1H), 7.61 (d, J = 7.62 Hz, 1H), 7.51–7.46 (m, 3H), 7.10 (t, J = 7.55 Hz, 1H), 6.86 (t, J = 8.90 Hz, 2H), 4.79 (s, 2H), 3.61 (t, J = 4.30 Hz, 2H), 3.57 (t, J = 4.30 Hz, 2H), 3.49–3.45 (m, 4H); ^{13}C NMR (100 MHz, DMSO–d_6): δ 166.69, 166.28, 158.48, 155.37, 155.16, 153.76, 139.54, 134.04, 131.92, 128.00, 122.44 (2C), 122.12, 122.00, 119.60, 114.92 (2C), 104.84, 70.25, 66.71, 66.55, 45.32, 42.09. HRMS (ESI$^+$) for $C_{23}H_{23}ClN_6O_5$, $[M+Na]^+$ calcd: 521.1311, found: 521.1288.

4.2.8. 2-((5-chloro-2-((4-(2-morpholinoacetamido)phenyl)amino) pyrimidin-4-yl)amino)-N-hydroxy benzamide (**9h**)

Yield 60.3%; off-white solid; dichloromethane/methanol: 12/1 (v/v). ^{1}H NMR (400 MHz, DMSO–d_6): δ 11.52 (s, 1H), 11.17 (s, 1H), 9.64 (s, 1H), 9.43 (s, 1H), 9.35 (s, 1H), 8.70 (s, 1H), 8.22 (s, 1H), 7.62 (d, J = 7.68 Hz, 1H), 7.58 (d, J = 8.52 Hz, 2H), 7.52 (t, J = 8.70 Hz, 2H), 7.49 (t, J = 7.86 Hz, 1H), 7.14 (t, J = 7.49 Hz, 1H), 3.65 (t, J = 4.02 Hz, 4H), 3.11 (s, 2H), 2.53–2.51 (m, 4H); ^{13}C NMR (100 MHz, DMSO–d_6): δ 168.07, 166.33, 158.27, 155.42, 155.20, 139.51, 136.36, 133.40, 131.90, 128.09, 122.63, 122.18, 120.49 (2C), 120.39 (2C), 119.83, 105.20, 66.56 (2C), 62.50, 53.71 (2C). HRMS (ESI$^+$) for $C_{23}H_{24}ClN_7O_4$, $[M+Na]^+$ calcd: 520.1471, found: 520.1448.

4.2.9. 1-(4-((5-chloro-4-((2-(methylcarbamoyl)phenyl)amino) pyrimidin-2-yl)amino)phenyl)-N-hydroxypiperidine-4-carboxamide (**9i**)

Yield 58.2%; off-white solid; dichloromethane/methanol: 8/1 (v/v). ^{1}H NMR (400 MHz, DMSO–d_6): δ 11.60 (s, 1H), 10.47 (s, 1H), 9.21 (s, 1H), 8.76–8.73 (m, 3H), 8.16 (s, 1H), 7.74 (d, J = 7.80 Hz, 1H), 7.48–7.45 (m, 3H), 7.12 (t, J = 7.62 Hz, 1H), 6.88 (d, J = 8.88 Hz, 2H), 3.63 (d, J = 12.24 Hz, 2H), 2.80 (d, J = 4.44 Hz, 3H), 2.60(td, J = 11.94, 2.52 Hz, 2H), 2.16–2.11 (m, 1H), 1.76–1.68 (m 4H); ^{13}C NMR (100 MHz, DMSO–d_6): δ 171.90, 169.44, 158.54, 155.42, 155.13, 147.23, 139.94, 132.52, 131.99, 128.41, 122.29, 121.84 (2C), 121.77, 120.97, 116.80 (2C), 104.73, 49.67 (2C), 39.65, 28.58 (2C), 26.81. HRMS (ESI$^+$) for $C_{24}H_{26}ClN_7O_3$, $[M+H]^+$ calcd: 496.1842, found: 496.1858.

4.2.10. 1-(4-((5-chloro-4-((2-(methylcarbamoyl)phenyl)amino) pyrimidin-2-yl)amino)benzyl)-N-hydroxypiperidine-4-carboxamide (**9j**)

Yield 61.7%; off-white solid; dichloromethane/methanol: 8/1 (v/v). ^{1}H NMR (400 MHz, DMSO–d_6): δ 11.60 (s, 1H), 10.39 (s, 1H), 9.44 (s, 1H), 8.78–8.74 (m, 2H), 8.68 (s, 1H), 8.21 (s, 1H), 7.75 (d, J = 7.44 Hz, 1H), 7.58 (d, J = 7.15 Hz, 2H), 7.46 (t, J = 7.30 Hz, 1H), 7.17 (d, J = 7.63 Hz, 2H), 7.14 (t, J = 7.32 Hz, 1H), 3.38 (s, 2H), 2.84–2.82 (m, 2H), 2.81 (s, 3H), 1.98–1.93 (m, 1H), 1.86 (t, J = 10.25 Hz, 2H), 1.63–1.56 (m 4H); ^{13}C NMR (100 MHz, DMSO–d_6): δ 172.04, 169.40, 158.28, 155.47, 155.12, 139.79, 139.41, 132.21, 131.88, 129.39 (2C), 128.46, 122.42, 121.94, 121.23, 120.13 (2C), 105.46, 62.48, 53.04 (2C), 40.00, 28.95 (2C), 26.81. HRMS (ESI$^+$) for $C_{25}H_{28}ClN_7O_3$, $[M+H]^+$ calcd: 532.1834, found: 532.1815.

4.2.11. 1-(3-(4-((5-chloro-4-((2-(methylcarbamoyl)phenyl)amino) pyrimidin-2-yl)amino)phenoxy) propyl)-N-hydroxypiperidine-4-carboxamide (**9k**)

Yield 69.8%; off-white solid; dichloromethane/methanol: 10/1 (v/v). ^{1}H NMR (400 MHz, DMSO–d_6): δ 11.59 (s, 1H), 10.39 (s, 1H), 9.27 (s, 1H), 8.77–8.67 (m, 3H), 8.17 (s, 1H), 7.74 (d, J = 7.14 Hz, 1H), 7.51 (d, J = 7.02 Hz, 2H), 7.46 (t, J = 7.25 Hz, 1H), 7.13 (d, J = 6.60 Hz, 2H), 6.85 (d, J = 8.22 Hz, 2H), 3.96 (t, J = 5.70 Hz, 2H), 2.90 (d, J = 5.70 Hz, 2H), 2.80 (d, J = 2.82 Hz, 3H), 2.43–2.39 (m, 2H), 1.98–1.94 (m, 1H), 1.88–1.83 (m, 4H), 1.64–1.56 (m 4H); ^{13}C NMR (100 MHz, DMSO–d_6): δ 171.79, 169.40, 158.48, 155.41, 155.11, 154.42, 139.86, 133.65, 131.91, 128.41, 122.30, 122.17 (2C), 121.77, 121.04, 114.74 (2C), 104.93, 66.48, 55.16, 53.30 (2C), 40.00, 28.90 (2C), 26.78, 26.82. HRMS (ESI$^+$) for $C_{27}H_{32}ClN_7O_4$, $[M+H]^+$ calcd: 554.2277, found: 554.2272.

4.2.12. 2-((5-chloro-2-((4-(2-(hydroxyamino)-2-oxoethoxy) phenyl)amino)pyrimidin-4-yl)amino)-N-hydroxybenzamide (**9l**)

Yield 69.6%; off-white solid. Ar atmosphere, **15g** (1.0 mmol) and hydroxylamine (20 mmol) in anhydrous methanol, sodium methoxide (25 mmol) in methanol solution was slowly added to the mixture. After the addition, the reaction was allowed to warm room temperature and stirred for 12 h. Adjusted pH to 6 with dilute hydrochloric acid, the inorganic salt was removed by filtration and the rest of organic phase was vacuum distilled to produce the **9l**. ^{1}H NMR (400 MHz, DMSO–d_6): δ 11.52 (s, 1H), 11.15 (s, 1H), 10.84 (s, 1H), 9.36 (s, 1H), 9.32 (s, 1H), 8.98 (s, 1H), 8.68 (s, 1H), 8.18 (s, 1H), 7.61 (d, J = 7.56 Hz, 1H), 7.52 (d, J = 8.28 Hz, 2H), 7.49 (t, J = 7.44 Hz, 1H), 7.12 (t, J = 7.26 Hz, 1H), 6.89 (t, J = 8.76 Hz, 2H), 4.43 (s, 2H); ^{13}C NMR (100 MHz, DMSO–d_6): δ 166.37, 165.00, 158.48, 155.44, 155.23, 153.58, 139.54, 134.36, 132.04, 128.07, 122.63, 122.10, 122.04 (2C), 119.73, 115.08 (2C), 104.95, 66.76. HRMS (ESI$^+$) for $C_{19}H_{17}ClN_6O_5$, $[M-H]^-$ calcd: 443.0876, found: 443.0874.

4.2.13. 2-((5-chloro-2-((4-(2-morpholino-2-oxoethoxy)phenyl) amino)pyrimidin-4-yl)amino)benzoic acid (**9m**)

Yield 62.1%; off-white solid. **15g** (100 mg) and 10% aq. Sodium hydroxide in 1,4-dioxane/water, the mixture was stirred at room temperature for 5 h. After reaction, adjusted pH to 6 with dilute hydrochloric acid and distilled out 1,4-dioxane. Then, the precipitate was filtrated and washed with water to obtain **9m** which could directly be used without further purification. ^{1}H NMR (400 MHz, DMSO–d_6): δ 11.48 (s, 1H), 9.33 (s, 1H), 8.92 (s, 1H), 8.21 (s, 1H), 8.03 (d, J = 7.52 Hz, 1H), 7.55 (t, J = 7.60 Hz, 1H), 7.51 (d, J = 8.76 Hz, 2H), 7.12 (t, J = 7.60 Hz, 1H), 6.90 (d, J = 8.77 Hz, 2H), 4.80 (s, 2H), 3.63–3.52 (m, 4H), 3.51–3.45 (m 4H); ^{13}C NMR (100 MHz, DMSO–d_6): δ 170.50, 166.82, 158.57, 155.51, 155.31, 153.79, 142.16, 134.40, 134.12, 131.78, 123.57, 122.56 (2C), 121.11, 116.36, 114.88 (2C), 105.29, 66.80, 66.67 (2C), 45.43, 42.22. HRMS (ESI$^+$) for $C_{23}H_{22}ClN_5O_5$, $[M-H]^-$ calcd: 482.1237, found: 482.1225.

4.2.14. Ethyl 2-((5-chloro-2-((4-(2-morpholino-2-oxoethoxy) phenyl)amino)pyrimidin-4-yl)amino) benzoate (**15g**)

Yield 55.3%; off-white solid. ^{1}H NMR (400 MHz, DMSO–d_6): δ 10.98 (s, 1H), 9.38 (s, 1H), 8.88 (s, 1H), 8.22 (s, 1H), 8.03(dd, J = 7.92, 1.24 Hz, 1H), 7.59 (t, J = 7.96 Hz, 1H), 7.50 (d, J = 8.68 Hz, 2H), 7.15 (t, J = 7.68 Hz, 1H), 6.88 (d, J = 8.68 Hz, 2H), 4.80 (s, 2H), 4.36 (q, J = 7.04 Hz, 2H), 3.63–3.54 (m, 4H), 3.50–3.44(m 4H), 1.33 (t, J = 7.04 Hz, 3H); ^{13}C NMR (100 MHz, DMSO–d_6): δ 168.07, 166.71, 158.49, 155.41 (2C), 153.91, 141.64, 134.54, 133.96, 131.26, 122.39 (3C), 121.60, 116.14, 114.97 (2C), 105.06, 66.77, 66.56 (2C), 61.81, 45.33, 42.10, 14.46. HRMS (ESI$^+$) for $C_{25}H_{26}ClN_5O_5$, $[M+Na]^+$ calcd: 534.1515, found: 534.1522.

4.3. Kinase enzymatic assays

The ADP-Glo™ system (EGFR^{WT}, Catalog. V9261; EGFR$^{T790M/L858R}$, Catalog. V5325) were purchased from Promega Corporation (USA) and were used to perform the enzymatic assays. The experiments were performed according to the instructions of the manufacturer. The more detailed and complete protocols, and the active kinase data were available at: https://www.promega.com.cn/resources/protocols/product-information-sheets/n/EGFR-kinase-enzyme-system-protocol/. For all of the tested targets, concentrations consisting of suitable levels from 0.1 to 1000 nM were used. The test was performed in a 384-well plate, and includes the major steps below: (1) perform 5 μL kinase reaction using 1 × kinase buffer (e.g., 1 × reaction buffer A), (2) incubate at room temperature

for 60 min, (3) add 5 μL of ADP-Glo™ reagent to stop the kinase reaction and deplete the unconsumed ATP leaving only ADP and a very low background of ATP, (4) incubate at room temperature for 40 min, (5) add 10 μL of kinase detection, (6) reagent to convert ADP to ATP and introduce luciferase and luciferin to detect ATP, (7) incubate at room temperature for 30 min, (8) plate was measured on TriStar® LB942 Multimode Microplate Reader (BERTHOLD) to detect the luminescence (Integration time 0.5–1 s). Curve fitting and data presentations were performed using GraphPad Prism version 5.0.

4.4. Cell activity assay

A 431, A 549, Aspc-1, and H 23 cells were obtained from the American Type Culture Collection. H 1975, HBE and L-02 cells were purchased from Fuheng Biology Company (Shanghai, China). H 1975, Aspc-1, H 23, and A 549 cells were grown in RPMI-1640 (Gibco®, USA) supplemented with 10% FBS (Gibco®, USA), 1% penicillin-streptomycin (Beyotime Company, China). A 431, HBE and L-02 cells were grown in DMEM (Gibco®, USA) supplemented with 10% FBS (Gibco®, USA), 1% penicillin-streptomycin (Beyotime Company, China). All cells were maintained and propagated as monolayer cultures at 37 °C in humidified 5% CO_2 incubator. The Cell Counting Kit-8 (CCK-8) reagent was purchased from Biotool Company (Switzerland). Cell viability was assessed by the CCK-8 assay based on the reduction of CCK-8 by succinate dehydrogenases of viable cells to a yellow formazan product. Cells were grown in 96-well culture plates (3000–4000/well) for 12 h before compounds of various concentrations (1.25–40 μM) were added. Cell proliferation was determined after treatment with compounds for 72 h. Subsequently, 10 μL of CCK-8 reagent (Biotool Company, Switzerland, 5.0 mg/mL) dissolved in the medium was added and the cells were incubated for another 1–2 h at 37 °C. The absorbance was measured at 450 nm with a microplate reader (Thermo Fisher, USA). All doses were tested in triplicates and the experiment was repeated at least three times. IC_{50} values were calculated using GraphPad Prism version 5.0.

4.5. Wound-healing assay

The cancer cells were cultured in 6-well plates for 48 h at 37 °C. The injury lines were created in the cell monolayer and washed with PBS to remove cell debris, then the cells were treated with **9d** (0.5 and 2 μM) for 0, 24, and 48 h. After that, the dead cells were washed away with PBS, and the images were photographed by the fluorescence microscope (OLYMPUS, Tokyo, Japan).

4.6. DAPI staining assays

Approximately 2×10^5 cells/well of H1975 cells in 6-well plates were incubated in an incubator for 12 h, then treated with different concentrations of inhibitors (0.125, 0.5, and 2 μM) for 72 h. After incubation, the cells were washed with PBS twice. DAPI staining was performed after being treated as mentioned above. The cells plated in 6-well plates were washed twice with PBS and fixed with 10% formaldehyde for 10 min, then washed with PBS three times. Cells were subsequently incubated in DAPI (1.0 μg/mL) solution at room temperature for 10 min, washed with PBS and examined under a fluorescence microscope (OLYMPUS, Tokyo, Japan).

4.7. Flow cytometry assay

The Annexin V-FITC Apoptosis Detection Kit and Cell Cycle Assay were all purchased from Beyotime Company (Shanghai, China). Compounds-induced apoptotic cell death was further quantitated by Annexin V-propidium iodide assay. Briefly, after treatment with different concentrations of compounds for 48 h, the cells were collected and washed twice with ice-cold PBS, cells then resuspended in binding buffer with Annexin-V and PI and incubated at room temperature for 15 min in the dark. The stained cells were analyzed using flow cytometry (Beckman, USA). The H1975 (1×10^6 cells/well) incubated in 6-well plates were treated with solvent control (DMSO), **9d** in medium containing 5% FBS for 72 h. Then, collected and fixed with 70% ethanol at 4 °C overnight. After being fixed with 70% ethanol at 4 °C, the cells were stained with Annexin V-FITC (5 μL)/propidium iodide (5 μL), and analyzed by flow cytometry assay (Becton-Dickinson, USA).

Cell cycle distribution was evaluated by flow cytometry. The cells at a density of approximately 2×10^5 cells/well were incubated in 6-well plates, treated with different concentrations of **9d** for 48 h, collected and fixed with 70% ice-cold ethanol at 4 °C overnight. Following this, cells were stained with 500 μL PBS containing 50 mg/mL propidium iodide and 0.5 mg/mL RNase for 30 min at 37 °C. The DNA content was analyzed on a flow cytometer (Beckman, USA).

4.8. Western blotting assay

The H1975 (2×10^5 cells/well) were plated in 6-well plates and treated with **9d** (0.5 and 1 μM) for 48 h. Then, the cells were washed twice times with PBS and lysed in a RIPA lysis buffer containing phenylmethanesulfonyl fluoride (PMSF). The lysate was centrifuged at 14,000 rpm for 15 min at 4 °C. The proteins were separated by SDS-PAGE (10–15%) and electrophoretically transferred to PVDF membranes. The blots were incubated in 1 × TBST containing 5% non-fat dry milk for 2 h to block nonspecific binding sites and incubated overnight at 4 °C with primary antibodies. Then the blots were incubated with horseradish peroxidase-conjugated antibodies (1:4000 dilution) for 1 h at room temperature after washing. Proteins were determined based on the enhanced chemiluminescence (ECL) method and images were taken using the Bio-Spectrum Gel Imaging System (UVP, USA).

4.9. Pharmacokinetic

Male Sprague-Dawley (SD) rats, weighing 200 ± 20 g, were used to study in vivo pharmacokinetics. All animal experiments were approved by the Animal Care and Use Committee of Dalian Medical University. The animals were maintained at 25 ± 2 °C and 50–60% relative humidity (RH) under natural light/dark conditions for 1 week before the experiment. Six rats were administered by tail vein injection (9d, 25 mg/kg). Blood samples were collected from the retro-orbital plexus under mild anesthesia into micro centrifuge tubes containing heparin (40 IU/ml blood) at different time points (10 min, 20 min, 40 min, 1 h, 2 h, 3 h, 4 h, 6 h, 8 h, 12 h and 24 h). Plasma was separated by centrifuging the blood samples at 7000 rpm for 5 min and stored at −20 °C prior to analysis.

The content of 9d in rat plasma was measured with a LC-MS/MS system. The plasma samples (200 μL) were mixed with ethyl acetate for extraction. The mixture was vortexed for 3 min and centrifuged at 4500 rpm for 5 min. The supernatant was dried under nitrogen, and the residue was re-dissolved with mobile phase. The de-clustering potential (DP) and the entrance potential (EP) were set at 55 V and 10 V. The collision voltage (CE) and the collision exit potential (CXP) were set at 30 eV and 40 V, respectively. Pharmacokinetic parameters were obtained using the DAS 2.1.1 software (Shanghai, China). The mass transition ion-pair was selected as m/z 485.3 → 452.3.

Declaration of competing interest

The authors declare that they have no known competing financial interests or personal relationships that could have appeared to influence the work reported in this paper.

Acknowledgements

This work was supported by the "innovative research team in SYPHU by the supporting fund for universities from the Chinese Central Government (51150039)", Research Fund of Higher Education of Liaoning Province (LQ2019004), Science and Technology Innovation Fund of Dalian, Liaoning province, China (2020JJ27SN072), “Xing Liao” Talents Project of Liaoning Province, China (XLYC1807011), Liaoning Province Ph.D. Research Start-up Fund (2020-BS-199), and Scientific Research Fund of Liaoning Province Education Administration (LZ2020041).

Appendix A. Supplementary data

Supplementary data to this article can be found online at https://doi.org/10.1016/j.ejmech.2021.113626.

References

[1] C.N. Prabhakar, Epidermal growth factor receptor in non-small cell lung cancer, Transl. Lung Cancer Res. 4 (2015) 110–118.
[2] N.E. Hynes, H.A. Lane, ERBB receptors and cancer: the complexity of targeted inhibitors, Nat. Rev. Canc. 5 (2005) 341–354.
[3] C.Y. Yang, J.C. Yang, P.C. Yang, Precision management of advanced non-small cell lung cancer, Annu. Rev. Med. 71 (2020) 117–136.
[4] S. Sun, J.H. Schiller, A.F. Gazdar, Lung cancer in never smokers–a different disease, Nat. Rev. Canc. 7 (2007) 778–790.
[5] Z. Yang, N. Yang, Q. Ou, Y. Xiang, T. Jiang, X. Wu, H. Bao, X. L Tong, X. N Wang, Y.W. Shao, Y.P. Liu, Y. Wang, C.C. Zhou, Investigating novel resistance mechanisms to third-generation EGFR tyrosine kinase inhibitor osimertinib in non-small cell lung cancer patients, Clin. Canc. Res. 24 (2018) 3097–3107.
[6] T.J. Lynch, D.W. Bell, R. Sordella, S. Gurubhagavatula, R.A. Okimoto, B.W. Brannigan, P.L. Harris, S.M. Haserlat, J.G. Supko, F.G. Haluska, D.N. Louis, D.C. Christiani, J. Settleman, D.A. Haber, Activating mutations in the epidermal growth factor receptor underlying responsiveness of non-small-cell lung cancer to gefitinib, N. Engl. J. Med. 350 (2004) 2129–2139.
[7] P. Bonomi, Erlotinib: a new therapeutic approach for non-small cell lung cancer, Expet Opin. Invest. Drugs 12 (2003) 1395–1401.
[8] D. Li, L. Ambrogio, T. Shimamura, S. Kubo, M. Takahashi, L.R. Chirieac, R.F. Padera, G.I. Shapiro, A. Baum, F. Himmelsbach, W.J. Rettig, M. Meyerson, F. Solca, H. Greulich, K.K. Wong, BIBW2992, an irreversible EGFR/HER2 inhibitor highly effective in preclinical lung cancer models, Oncogene 27 (2008) 4702–4711.
[9] O. Kalous, D. Conklin, A.J. Desai, N.A. O'Brien, C. Ginther, L. Anderson, D.J. Cohen, C.D. Britten, I. Taylor, J.G. Christensen, D.J. Slamon, R.S. Finn, Dacomitinib (PF-00299804), an irreversible pan-HER inhibitor, inhibits proliferation of HER2-amplified breast cancer cell lines resistant to trastuzumab and lapatinib, Mol. Canc. Therapeut. 11 (2012) 1978–1987.
[10] M.L. Sos, H.B. Rode, S. Heynck, M. Peifer, F. Fischer, S. Klüter, V.G. Pawar, C. Reuter, J.M. Heuckmann, J. Weiss, L. Ruddigkeit, M. Rabiller, M. Koker, J.R. Simard, M. Getlik, Y. Yuza, T.H. Chen, H. Greulich, R.K. Thomas, D. Rauh, Chemogenomic profiling provides insights into the limited activity of irreversible EGFR inhibitors in tumor cells expressing the T790M EGFR resistance mutation, Canc. Res. 70 (2010) 868–874.
[11] Y.W. Kim, J.H. Ko, Z.Y. Cui, A. Abolhoda, J.S. Ahn, S.H. Ou, MyJ. Ahn, K. Park, The EGFR T790M mutation in acquired resistance to an irreversible SecondGeneration EGFR inhibitor [J], Canc. Ther. 11 (2012) 784–791.
[12] W. Zhou, D. Ercan, L. Chen, C.H. Yun, D. Li, M. Capelletti, A.B. Cortot, L. Chirieac, R.E. Iacob, R. Padera, J.R. Engen, K.K. Wong, M.J. Eck, N.S. Gray, P.A. Janne, Novel mutant-selective EGFR kinase inhibitors against EGFR T790M, Nature 462 (2009) 1070–1074.
[13] M.R. Finlay, M. Anderton, S. Ashton, P. Ballard, P.A. Bethel, M.R. Box, R.H. Bradbury, S.J. Brown, S. Butterworth, A. Campbell, C. Chorley, N. Colclough, D.A. Cross, G.S. Currie, M. Grist, L. Hassall, G.B. Hill, D. James, M. James, P. Kemmitt, T.K. linowska, G. Lamont, S.G. Lamont, N. Martin, H.L. McFarland, M.J. Mellor, J.P. Orme, D. Perkins, P. Perkins, G. Richmond, P. Smith, R.A. Ward, M.J. Waring, D. Whittaker, S. Wells, G.L. Wrigley, Discovery of a potent and selective EGFR inhibitor (AZD9291) of both sensitizing and T790M resistance mutations that spares the wild type form of the receptor, J. Med. Chem. 57 (2014) 8249–8267.
[14] D.A. Cross, S.E. Ashton, S. Ghiorghiu, C. Eberlein, C.A. Nebhan, P.J. Spitzler, J.P. Orme, M.R. Finlay, R.A. Ward, M.J. Mellor, G. Hughes, A. Rahi, V.N. Jacobs, M.R. Brewer, E. Ichihara, J. Sun, H. Jin, P. Ballard, K. Al-Kadhimi, R. Rowlinson, T. Klinowska, G.H. Richmond, M. Cantarini, D.W. Kim, M.R. Ranson, W. Pao, AZD9291, an irreversible EGFR TKI, overcomes T790M-mediated resistance to EGFR inhibitors in lung cancer, Canc. Discov. 4 (2014) 1046–1061.
[15] Z. Piotrowska, M.J. Niederst, C.A. Karlovich, H.A. Wakelee, J.W. Neal, M. Mino-Kenudson, L. Fulton, A.N. Hata, E.L. Lockerman, A. Kalsy, S. Digumarthy, A. Muzikansky, M. Raponi, A.R. Garcia, H.E. Mulvey, M.K. Parks, R.H. DiCecca, D. Dias-Santagata, A.J. Iafrate, A.T. Shaw, A.R. Allen, J.A. Engelman, L.V. Sequist, Heterogeneity underlies the emergence of EGFRT790 wild-type clones following treatment of T790M-positive cancers with a thirdgeneration EGFR inhibitor, Canc. Discov. 5 (2015) 713–722.
[16] M.J. Niederst, H. Hu, H.E. Mulvey, E.L. Lockerman, A.R. Garcia, Z. Piotrowska, L.V. Sequist, J.A. Engelman, The allelic context of the C797S mutation acquired upon treatment with third-generation EGFR inhibitors impacts sensitivity to subsequent treatment strategies, Clin. Canc. Res. 21 (2015) 3924–3933.
[17] C.A. Eberlein, D. Stetson, A.A. Markovets, K.J. Al-Kadhimi, Z. Lai, P.R. Fisher, C.B. Meador, P. Spitzler, E. Ichihara, S.J. Ross, M.J. Ahdesmaki, A. Ahmed, L.E. Ratcliffe, E.L.C. O'Brien, C.H. Barnes, H. Brown, P.D. Smith, J.R. Dry, G. Beran, K.S. Thress, B. Dougherty, W. Pao, D.A.E. Cross, Acquired resistance to the mutant-selective EGFR inhibitor AZD9291 is associated with increased dependence on RAS signaling in preclinical models, Canc. Res. 75 (2015) 2489–2500.
[18] Q.N. Li, T. Zhang, S.L. Li, L.J. Tong, J.Y. Li, Z.C. Su, F. Feng, D.H. Sun, Y. Tong, X. Wang, Z.J. Zhao, L.L. Zhu, J. Ding, H.L. Li, H. Xie, Y.F. Xu, Discovery of potent and noncovalent reversible EGFR kinase inhibitors of egfrl858r/t790m/C797S, J. Med. Chem. 10 (2019) 869–873.
[19] B. Sever, M.D. Altıntop, M.O. Radwan, A. Özdemir, M. Otsuka, M. Fujita, H.I. Ciftci, Design, synthesis and biological evaluation of a new series of thiazolyl-pyrazolines as dual EGFR and HER2 inhibitors, Eur. J. Med. Chem. 182 (2019) 111648.
[20] M. Ai, C.Y. Wang, Z.Y. Tang, K.X. Liu, X.L. Sun, T.Y. Ma, Y.X. Li, X.D. Ma, L. Li, L.X. Chen, Design and synthesis of diphenylpyrimidine derivatives (DPPYs) aspotential dual EGFR T790M and FAK inhibitors against a diverse range of cancer cell lines, Bioorg. Chem. 94 (2020) 103408.
[21] Y.M. Zhu, X. Zheng, C.Y. Wang, X.L. Sun, H.J. Sun, T.Y. Ma, Y.X. Li, K.X. Liu, L.X. Chen, X.D. Ma, Synthesis and biological activity of thieno[3,2-d]pyrimidines as potent JAK3 inhibitors for the treatment of idiopathic pulmonary fibrosis, Bioorg. Med. Chem. 28 (2020) 115254.
[22] F.Y. Chi, L.X. Chen, C.Y. Wang, L. Li, X. L Sun, Y.J. Xu, T.Y. Ma, K.X. Liu, X.D. Ma, X.H. Shu, JAK3 inhibitors based on thieno[3,2-d]pyrimidine scaffold: design, synthesis and bioactivity evaluation for the treatment of B-cell lymphoma, Bioorg. Chem. 95 (2020) 103542.
[23] Q. Shi, A.B. Hjelmeland, S.T. Keir, L. Song, S. Wickman, D. Jackson, O. Ohmori, D.D. Bigner, H.S. Friedman, J.N. Rich, A novel low-molecular weight inhibitor of focal adhesion kinase, TAE226, inhibits glioma growth, Mol. Carcinog. 46 (2007) 488–496.
[24] Z. Song, S. Huang, H. Yu, Y. Jiang, C. Wang, Q. Meng, X. Shu, H. Sun, K. Liu, Y. Li, X.D. Ma, Synthesis and biological evaluation of morpholine-substituted diphenylpyrimidine derivatives (Mor-DPPYs) as potent EGFR T790M inhibitors with improved activity toward the gefitinib-resistant non-small cell lung cancers (NSCLC), Eur. J. Med. Chem. 133 (2017) 329–339.